Research Article

Modeling and Simulations of Collapse Instabilities of Microbeams due to Capillary Forces

Hassen M. Ouakad and Mohammad I. Younis

Department of Mechanical Engineering, State University of New York at Binghamton, Binghamton, NY 13902, USA

Correspondence should be addressed to Mohammad I. Younis, myounis@binghamton.edu

We present modeling and analysis for the static behavior and collapse instabilities of doubly-clamped and cantilever microbeams subjected to capillary forces. These forces can be as a result of a volume of liquid trapped underneath the microbeam during the rinsing and drying process in fabrication. The model considers the microbeam as a continuous medium, the capillary force as a nonlinear function of displacement, and accounts for the mid-plane stretching and geometric nonlinearities. The capillary force is assumed to be distributed over a specific length underneath the microbeam. The Galerkin procedure is used to derive a reduced-order model consisting of a set of nonlinear algebraic and differential equations that describe the microbeams static and dynamic behaviors. We study the collapse instability, which brings the microbeam from its unstuck configuration to touch the substrate and gets stuck in the so-called pinned configuration. We calculate the pull-in length that distinguishes the free from the pinned configurations as a function of the beam thickness and gap width for both microbeams. Comparisons are made with analytical results reported in the literature based on the Ritz method for linear and nonlinear beam models. The instability problem, which brings the microbeam from a pinned to adhered configuration is also investigated. For this case, we use a shooting technique to solve the boundary-value problem governing the deflection of the microbeams. The critical microbeam length for this second instability is also calculated.

1. Introduction and Background

Wet etching of sacrificial layers to release microbeams from the substrate is an important step in the fabrication of many microelectromechanical systems (MEMS) structures and devices. During drying, the rinse liquid trapped underneath the microbeams creates strong capillary forces pulling them toward the substrate. Because of their large surface areas, those microbeams can permanently get stuck to the substrate if the capillary forces are greater than their restoring forces. If the resorting force of a microbeam cannot resist the capillary force, it collapses hitting the substrate. This is similar to the *pull-in* instability when the microbeam is
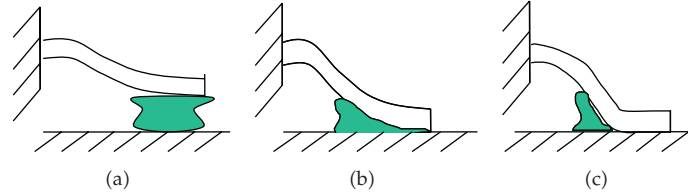
Figure 1: The possible scenarios for the configuration of a cantilever microbeam under the effect of capillary forces.

actuated by electrostatic forces [1–3]. In order for the microbeam to get stuck to the substrate, it needs to overcome another critical instability limit, which distinguishes microbeams that adheres to the substrate when collapsed from those that can pull back to their free position.

To clarify the various instabilities due to capillary forces, we consider as an example a cantilever microbeam with a volume of liquid trapped underneath it, Figure 1. The microbeam under the effect of capillary forces can take one of the following three configurations depending on its stiffness and the capillary force distribution.

(a) *Free-standing configuration.* The microbeam is not in contact with the substrate, Figure 1(a). In this case, it deflects and maintains equilibrium with the capillary force.

(b) *Pinned configuration.* In this case, the capillary force overcomes the stiffness of the cantilever beam causing it to collapse. One of the possible post-collapse scenarios is that the microbeam makes a contact with the substrate at its tip, where it is pinned and stuck. At this instance, the stiffness of the microbeam becomes capable of opposing the capillary force underneath; hence the microbeam stays in this configuration in equilibrium, Figure 1(b).

(c) *Adhered (stuck) configuration.* In this case, the capillary force is so strong that it overcomes the restoring force of the microbeam in configuration (Figure 1(b)) to bring it to configuration (Figure 1(c)), where part of the microbeam becomes adhered to the substrate. The contact length of the cantilever beam varies with the microbeam length, stiffness, and also with the distribution of the capillary force. This paper is concerned with analyzing the stability of doubly clamped and cantilever microbeams while going from the unstuck to pinned configuration (Figure 1(a) → Figure 1(b)) and from the pinned to the adhered one (Figure 1(b) → Figure 1(c)) of a cantilever beam.

There has been a major focus in literature on modeling structures under the effect of capillary forces. Some studies [4–6] attempted to extract the stiction force and predict microbeams behavior before and after collapse. In-use stictions after the dry process for microcantilevers were investigated experimentally in several works [4, 7]. Others studies [8–13] treated the stiction failure phenomena and described several modeling methods and approaches (surface interaction energy approach [8], vibration and dynamic fracture models [9], structural analysis methods [10, 11], and experimental models [12, 13]) to overcome this failure. The adhesion configuration was investigated experimentally [14], in which the transitions from initially undeformed cantilevers to pinned and adhered beams were quantified using a nanoindenter machine.

Instabilities that microbeams undergo under the effect of electrostatic forces, which are similar to those due to capillary forces, were treated in many studies [1, 2, 15, 16]. For example, Knapp and De Boer [15] developed a model of the adhesion problem of microcantilevers. The collapse problem due to electrostatic forces, called the pull-in phenomenon, was also investigated in several works for both clamped-clamped and

cantilever microbeams [1, 2]. Other studies [1, 16] analyzed the instabilities problems due to electrostatic forces beyond the pull-in phenomenon for simple microcantilevers.

Many studies also dealt with the problem of microstructure stiction under the effect of humidity. De Boer et al. [17] characterized the adhesion of surface micromachined polysilicon beams subject to controlled humidity ambient. They studied the effect of the relative humidity on the adhesion for these beams under equilibrium conditions. They demonstrated that adhesion increases exponentially with the relative humidity. De Boer and Michalske [18] demonstrated, using surface micromachined samples, the accurate measurement of cantilever beam adhesion by using test structures, which are adhered over long attachment lengths.

The collapse and adhesion problems due to capillary forces have been investigated for both cantilever and clamped-clamped microbeams [19–22]. Mastrangelo and Hsu [19, 20] applied energy methods and the Ritz technique on an Euler-Bernoulli beam model to determine critical lengths of microbeams, such as the pull-in length, in attempts to determine when a microstructure can collapse and get stuck. In the Ritz method, a single trial function was used in the model. They used both a linear and a nonlinear beam model, which accounts for the mid-plane stretching nonlinearity in doubly clamped microbeams. They compared between their theoretical results and experimental data for critical lengths of doubly clamped and cantilever microbeams where they showed good agreement among the results except for some data where the nonlinear behavior is strong. Legtenberg et al. [21] presented linear models and analysis to study the effect of capillary forces on the microbeams stability. They used approximate analytical technique (Rayleigh-Ritz method) based on one trial trigonometric function to study the effect of capillary forces on microbeams and how this could lead to collapse failures.

This paper focuses on microbeams, particularly doubly clamped (bridges) and cantilever, because of their common use in MEMS. By reviewing the state of the art, we can see that the collapse problem due to capillary forces has been investigated for both cantilever and clamped-clamped microbeams [19–22]. From these significant contributions, nondimensional numbers, such as the elastocapillary number, as well as critical lengths of microbeams, such as the pull-in length, were introduced in attempts to determine when a microstructure can collapse and get stuck and what can be done to improve its design to prevent stiction. However, the following can be observed on the theoretical work presented so far.

(i) The models and theoretical analysis were based on approximate analytical techniques, particularly the Ritz method. In this method, the deflection of the microbeam is approximated using a series of trial functions.

(ii) In the literature, a single function has been used in the Ritz series. This has been done without investigating if using a single term in the series leads to converged and accurate results.

(iii) There has been no investigation to whether the chosen trial function (algebraic or trigonometric) yields the most accurate prediction or if it is the best choice among other function types.

In previous works [1, 23, 24], we developed computational approaches (shooting technique, reduced-order models) to investigate the static and dynamic behavior of microbeams (clamped-clamped and cantilever) under the actuation of electrostatic loads. In this work we extend those approaches and reduced-order models to investigate the collapse problems of doubly clamped and cantilever microbeams due to capillary forces.
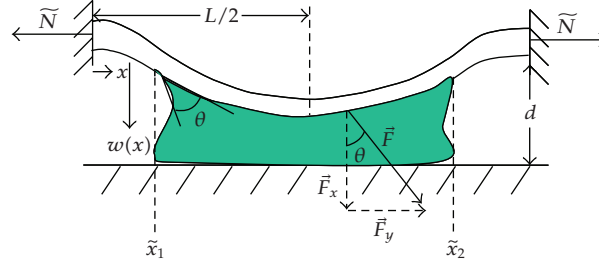
Figure 2: Schematic of the doubly clamped microbeam under the effect of capillary forces.

The organization of this paper is as follows. In Section 2, we study the collapse problem of a doubly clamped microbeam from the unstuck to the pinned configuration. In Section 3, we conduct a similar investigation for cantilever microbeams. Section 4 presents a model and analysis for the static behavior and collapse instability of cantilever microbeams while going from the pinned to the adhered configuration.

2. The Collapse Problem for a Clamped-Clamped Microbeam

In this section, we study the collapse problem of a doubly clamped microbeam due to a capillary force. This instability takes the microbeam from the unstuck configuration, Figure 1(a), to the pinned configuration, Figure 1(b).

2.1. Modeling

Figure 2 shows a doubly clamped microbeam with a droplet of liquid trapped underneath it inducing a capillary force. This force is partially distributed underneath the beam over its length between $\tilde{x}_1$ and $\tilde{x}_2$. The fluid has a surface tension γ and it forms an angle θ with both the beam and the substrate. Since both the beam and the substrate are made with the same material and they are considered to be highly hydrophilic surfaces, θ is taken to be zero for the beam-fluid and fluid-substrate interfaces (perfect wetting condition). The initial distance separating the microbeam from the substrate is d. The microbeam is modeled as a linear prismatic Euler-Bernoulli beam of width b, thickness h, length L, Young's modulus E, density ρ, cross section area $A = bh$, and area moment of inertia $I = bh^3/12$. We denote by $\widetilde{N}$ the induced axial load on the beam, which can be due to residual stresses. We let $w(x)$ be the beam displacement at location x. Note that the Meniscus effects are neglected.

For a given point on the beam-liquid and the liquid-substrate interface, there exists a local capillary force F_{cap} of a magnitude proportional to $\gamma\cos(\theta)$ (Young-Dupré equation [25]), and a direction perpendicular to the beam width z [25]. Assuming the microbeam and the underneath substrate can be treated as two parallel rigid plates; the capillary force per unit length acting on the microbeam can be expressed as $\overrightarrow{F} = \int_0^b \overrightarrow{F_{\mathrm{cap}}} \overrightarrow{dz}$. In addition, the capillary force is assumed to satisfy the following [25]:

   (i) The capillary force makes an angle θ with the unit vector that is normal to the surface of the fluid, where θ is the contact angle as shown in Figure 2.

(ii) The magnitude of the force $|\vec{F}|$ is given by $\gamma A_c / r$, where r is the distance between the microbeam and the substrate and A_c is the area of contact between the microbeam and the fluid. Under the action of capillary forces, the microbeam deflects changing the distance r, which in turns changes the magnitude of the capillary force. This will cause further deflection of the microbeam. This pattern continues until equilibrium is reached between the microbeam and the capillary force. To account for the change in r, we follow Legtenberg et al. [21] and modify the capillary force expression to become $F = 2\gamma b \cos(\theta)/(d - w)$.

In addition to these assumptions, we will not assume the volume of fluid trapped underneath the beam to be constant while the beam is being deflected. This implies that there will be some leakage of fluid across the beam width during its deflection.

Based on the above, the equation of motion and associated boundary conditions of the microbeam shown in **Figure 2** can be expressed as [21]

$$EI \frac{\partial^4 w}{\partial x^4} = \left[\frac{EA}{2L} \int_0^L \left(\frac{\partial w}{\partial x} \right)^2 dx + \widetilde{N} \right] \frac{\partial^2 w}{\partial x^2} + \frac{2\gamma b \cos\theta}{(d - w)} [u(x - \tilde{x}_1) - u(x - \tilde{x}_2)],$$

$$w(0) = w(L) = 0, \qquad \frac{\partial w}{\partial x}(0) = \frac{\partial w}{\partial x}(L) = 0,$$

(2.1)

where u is the Heaviside function.

For convenience, we introduce the following nondimensional variables:

$$\hat{w} = \frac{w}{d}; \qquad \hat{x} = \frac{x}{L}.$$

(2.2)

In nondimensional forms, and while dropping the hats, (2.1) become

$$\frac{\partial^4 w}{\partial x^4} = \left[\alpha_1 \int_0^1 \left(\frac{\partial w}{\partial x} \right)^2 dx + N \right] \frac{\partial^2 w}{\partial x^2} + \frac{\alpha_2}{(1 - w)} [u(x - x_1) - u(x - x_2)],$$

(2.3)

$$w(0) = 0, \qquad w(1) = 0, \qquad \frac{\partial w}{\partial x}(0) = 0, \qquad \frac{\partial w}{\partial x}(1) = 0,$$

(2.4)

where

$$\alpha_1 = 6 \left(\frac{d}{h} \right)^2, \qquad \alpha_2 = \frac{2\gamma b \cos(\theta) L^4}{EId^2}, \qquad N = \frac{\widetilde{N}L^2}{EI}, \qquad x_1 = \frac{\tilde{x}_1}{L}, \qquad x_2 = \frac{\tilde{x}_2}{L}.$$

(2.5)

Next, (2.3) and (2.4) are discretized using a Galerkin procedure to yield a reduced-order model (ROM) [23, 24]. First, (2.3) is multiplied by $(1 - w)$. Then we approximate the microbeam deflection as

$$w(x) = \sum_{i=1}^n a_i \phi_i(x)$$

(2.6)

where $\phi_i(x)$ $(i = 1, 2, \ldots, n)$ are the normalized mode shapes of the considered microbeam and a_i $(i = 1, 2, \ldots, n)$ are nontime varying constant coefficients. Because of the symmetric nature of a doubly clamped microbeam and the capillary forces, only symmetric (odd) mode shapes are used.

Substituting (2.6) into the resulting equation, multiplying by $\phi_i(x)$, using the orthogonality conditions of the mode shapes , and integrating numerically the outcome from 0 to 1, yields the reduced-order model:

$$
\int_0^1 \left\{ \left[1 - \sum_{i=1}^n a_i \phi_i(x) \right] \left[\sum_{i=1}^n u_i(t) \phi_i^{iv}(x) \right] \phi_j(x) dx \right\}
$$

$$
= \alpha_2 \int_0^1 \phi_j(x) [u(x - x_1) - u(x - x_2)] dx + \alpha_1 \left(\int_0^1 \left\{ \left[\sum_{i=1}^n a_i \phi_i'(x) \right]^2 \right\} dx + N \right) \qquad (2.7)
$$

$$
\times \left(\int_0^1 \left\{ \left[1 - \sum_{i=1}^n a_i \phi_i(x) \right] \left[\sum_{i=1}^n a_i \phi_i''(x) \right] \phi_j(x) dx \right\} \right), \quad j = 1, \ldots, n.
$$

The obtained ROM contains a system of nonlinear algebraic equations that can be solved numerically using Newton-Raphson method to obtain a_i and hence the static deflection of the microbeam.

2.2. Results

Next, results are presented for the static deflection of the doubly clamped microbeam due to capillary forces. First, the convergence of the ROM is examined as the number of modes is increased, that is, the number of modes needed in (2.6) for convergence is determined. We consider here a microbeam of $100\,\mu$m length, $10\,\mu$m width, $1.5\,\mu$m thickness, and a gap width underneath equals to $1.18\,\mu$m. Young's modulus is set equal to $169\,$GPa. The applied axial load N and the angle formed by the fluid and the microbeam are set equal to zero. The fluid surface tension is assumed to be equal to $0.073\,$N/m. Figure 3 shows the normalized maximum deflection of the considered microbeam using the ROM for different number of modes (first few) and while varying the capillary force distribution for the case of $x_1 = x_2$. It follows from Figure 3 that the use of three symmetric modes yields converged results. As seen from Figure 3, the microbeam exhibits collapse instability at a specific threshold of liquid volume, where the slope of the curve approaches infinity, as predicted by Mastrangelo and Hsu [19].

Next, we assume complete wetted area underneath the beam and calculate the length where a microbeam undergoes its first instability from the free to the pinned configuration (pull-in length). First, a linear beam theory is assumed; hence the nonlinear mid-plane stretching term in (2.3) is set equal to zero. To estimate the pull-in length, the static deflection of the microbeam is calculated for various beam lengths (Figure 4). When the slope of the maximum displacement-length curve approaches infinity, the length of the curve where it ends is identified as the pull-in length. At this instant, the eigenvalue of the static-problem approaches zero, similar to the case of electrostatic force [1, 23], indicating reaching the pull-in length. This procedure is repeated for various values of thicknesses h and gap widths d, which lumped in the parameter $(d^2 h^3)^{1/4}$ [19, 21].
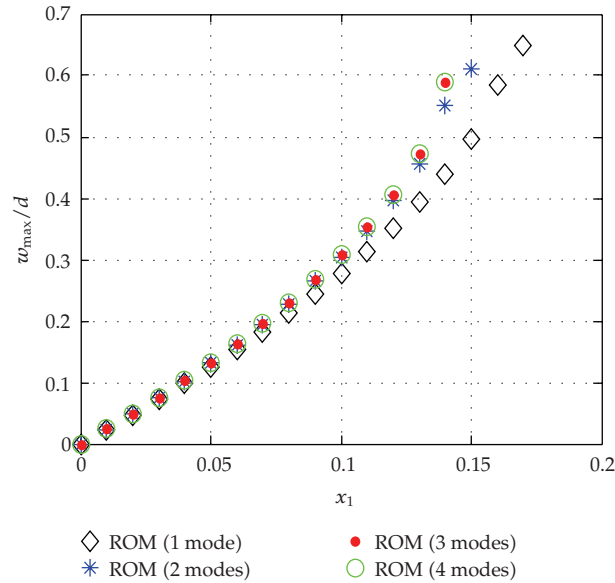
Figure 3: The normalized maximum deflection of the doubly clamped microbeam versus the normalized liquid distribution using the ROM for different number of modes. In the figure, a symmetric distribution for the liquid is assumed ($x_1 = x_2$). Here $\alpha_1 = 3.71$ and $\alpha_2 = 220.6$.
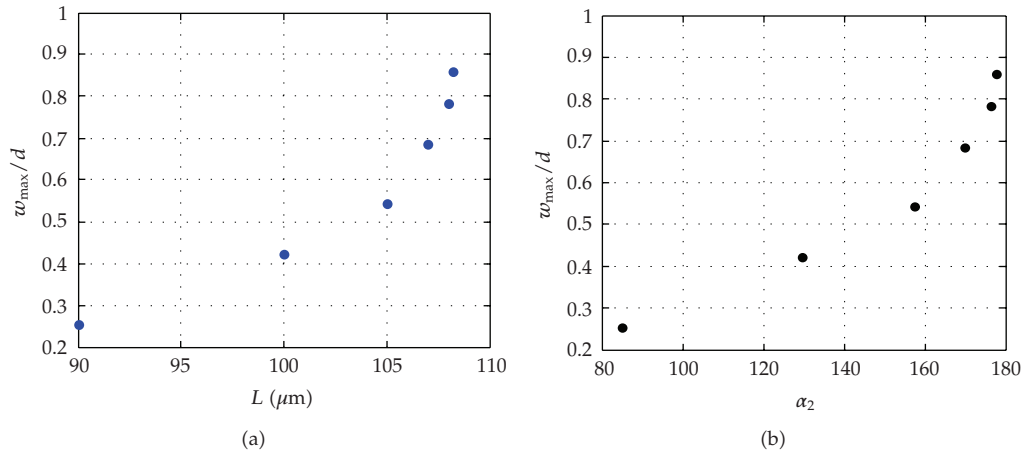

Figure 4: The normalized maximum deflection versus the beam length using the ROM (three modes) for completely wetted beam of $10\,\mu$m width for the case of $(d^2 h^3)^{1/4} = 2\,\mu$m$^{5/4}$. Here α_1 is equal to 1.5.

Mastrangelo and Hsu [19] and Legtenberg et al. [21] have derived analytical expressions for the pull-in length using an energy method, the Ritz method. They found this expression for the pull-in length $L_p = (3E/8\gamma)^{1/4}(d^2 h^3)^{1/4}$. This expression indicates linear dependence of the pull-in length on the parameter $(d^2 h^3)^{1/4}$. In Figure 5, we show the variation of the pull-in lengths using the ROM employing the first three symmetric modes and compare to those found by Mastrangelo and Hsu [19] and Legtenberg et al. [21]. As seen from the figure, there is a good agreement among all the results. This indicates that the
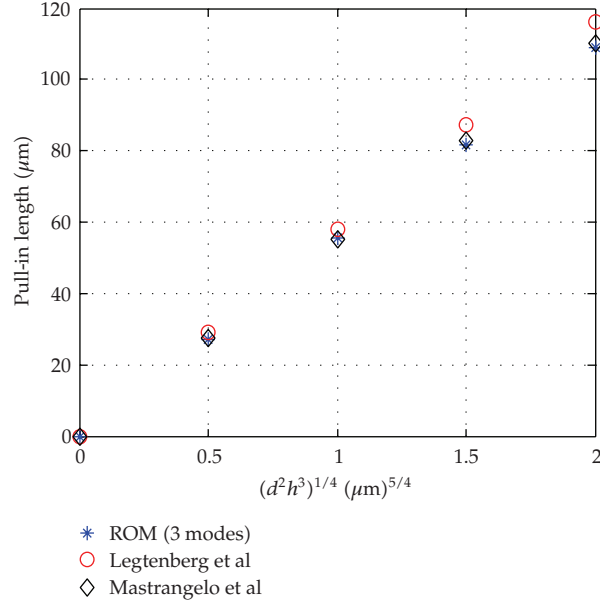
Figure 5: The pull-in length of the doubly clamped microbeam as a function of the parameter $(d^2h^3)^{1/4}$ without including the effect of mid-plane stretching.

analytical expression developed by Mastrangelo and Hsu [19] for the elastocapillary number, which is the base of the pull-in length calculations in [19, 21], yields fairly accurate results assuming linear behavior for the microbeam.

Next, we include the effect of mid-plane stretching in our model and compare the pull-in length calculated using the ROM (with one and three modes) with results obtained using the model of Mastrangelo and Hsu [19], which is based on a nonlinear beam model. The latter results are calculated by setting the elastocapillary number of Mastrangelo and Hsu [19], which accounts for mid-plane stretching, equal to unity and solve for the pull-in length. Figure 6 shows the results. Two cases are examined, one when varying the thickness of the microbeam while fixing the gap width (Figure 6(a)), and the other when varying the gap width while keeping the thickness fixed. We note from Figure 6 differences between our results and those calculated using the model of Mastrangelo and Hsu [19]. This might be attributed to the fact that using the Ritz method with one single trial function may not lead to converged results in inherently nonlinear regime. Further studying is needed in the future to investigate this difference.

Before ending this section, it is worth to comment about the assumption of our model that the volume of fluid underneath the beam varies such that the values of x_1 before the beam deflects and after it reaches equilibrium are the same. We believe that the actual scenario is in between this assumption and the assumption of constant volume of fluid underneath the beam, which allows x_1 to expand while the beam deflects (x_1 depends on w) to keep the total volume constant. Such an increase in x_1 means that the capillary forces acting on the microbeam will be in general larger than those used in this model. This will cause earlier instability and larger deflection of the microbeams compared to what has been predicted using our model and that of [19, 21]. To model such a problem, a sequential scheme may need to be built that can update the values of x_1 while the beam deflects.
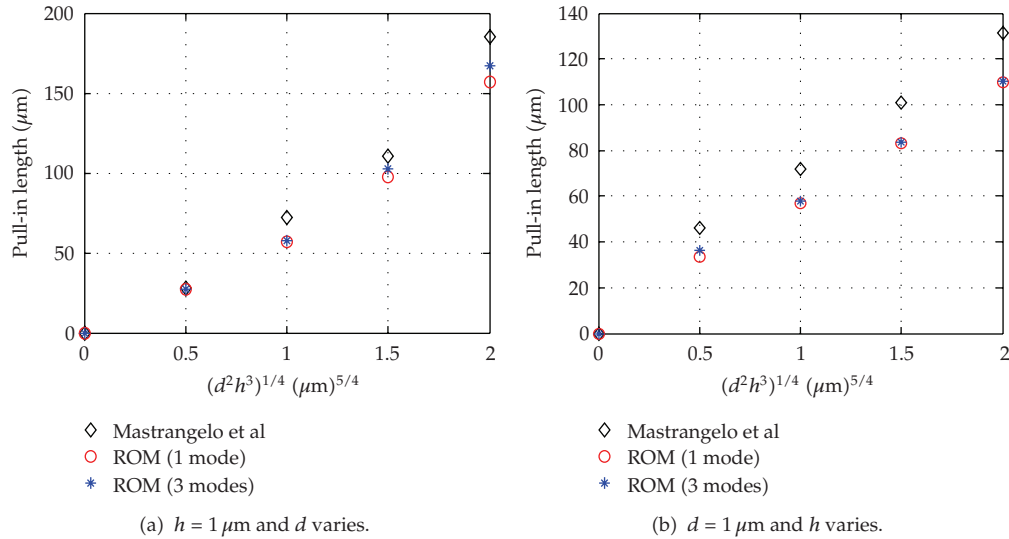
(a) $h = 1\,\mu$m and d varies.

(b) $d = 1\,\mu$m and h varies.

Figure 6: The pull-in length of the doubly clamped microbeam as a function of the parameter $\left(d^2h^3\right)^{1/4}$ including the effect of mid-plane stretching.
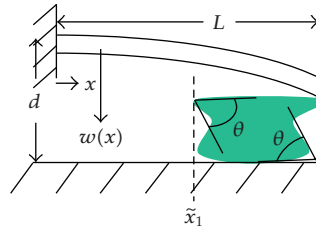

Figure 7: Schematic of the cantilever microbeam under the effect of capillary forces.

3. The Collapse Problem for a Cantilever Microbeam

In this section, we study the collapse problem of a cantilever microbeam due to a capillary force. There are number of differences distinguishing this microbeam from a doubly clamped one including the absence of mid-plane stretching and induced-residual stress. Those facts beside its very low stiffness make a cantilever microbeam more susceptible for collapse problems due to capillary forces.

3.1. Modeling

The cantilever microbeam shown in Figure 7 consists of an elastic beam with a volume of liquid underneath it, which induces capillary force. We will assume here the same geometric and physical parameters used to model the doubly clamped microbeam in Section 2.1.
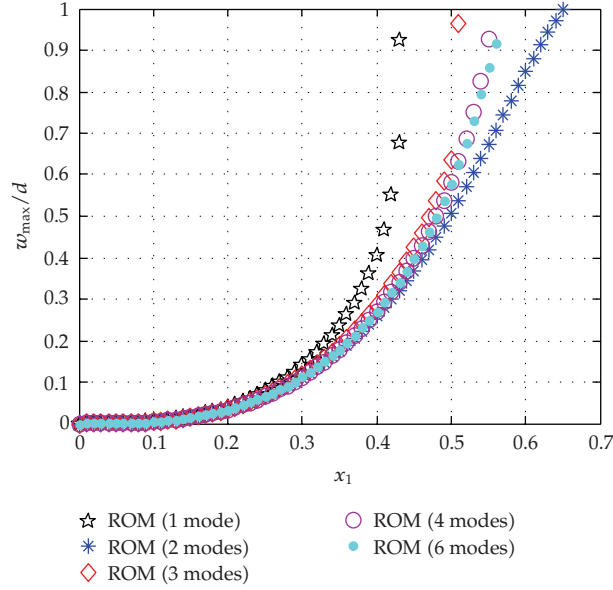
Figure 8: The normalized maximum deflection of the cantilever microbeam versus the normalized liquid distribution using the ROM for different number of modes. Here $\alpha_1 = 0$ and $\alpha_2 = 27.17$.

Using the same procedure and assumptions of Section 2.1, we end up with the following nondimensional equation of motion and its boundary conditions [26]:

$$\frac{\partial^4 w}{\partial x^4} = -\frac{\alpha_1}{6}\frac{\partial}{\partial x}\left[\frac{\partial w}{\partial x}\frac{\partial}{\partial x}\left(\frac{\partial w}{\partial x}\frac{\partial^2 w}{\partial x^2}\right)\right] + \frac{\alpha_2}{(1-w)}u(x - (1 - x_1)), \tag{3.1}$$

$$w(0) = 0, \qquad \frac{\partial w}{\partial x}(0) = 0, \qquad \frac{\partial^2 w}{\partial x^2}(1) = 0, \qquad \frac{\partial^3 w}{\partial x^3}(1) = 0, \tag{3.2}$$

where $x_1 = 1 - (\tilde{x}_1/L)$, α_1 and α_2 are as defined in (2.5).

Note that the first term on the right side of (3.1) is the cubic nonlinearity that results from geometry effect of the cantilever microbeam. Next, (3.1) and (3.2) are discretized using a Galerkin procedure to yield a ROM similar to Section 2.1. Here, we use the first few mode shapes (symmetric and antisymmetric) in the descritization (2.6).

3.2. Results

Here, we show results for the static deflection of the cantilever microbeam due to capillary forces. We first examine the convergence of the ROM, same as we did in Section 2.2 for the doubly clamped microbeam. We consider here a cantilever microbeam of 80 μm length, 10 μm width, 2.5 μm thickness, and a gap width underneath equals to 1 μm.

Figure 8 shows the normalized maximum deflection of the considered microbeam using the ROM for different number of modes and while varying the capillary force distribution x_1. It follows from Figure 8 that the use of four modes yields converged results. The nonmonotonic convergence of the ROM observed in Figure 8 might be attributed to the
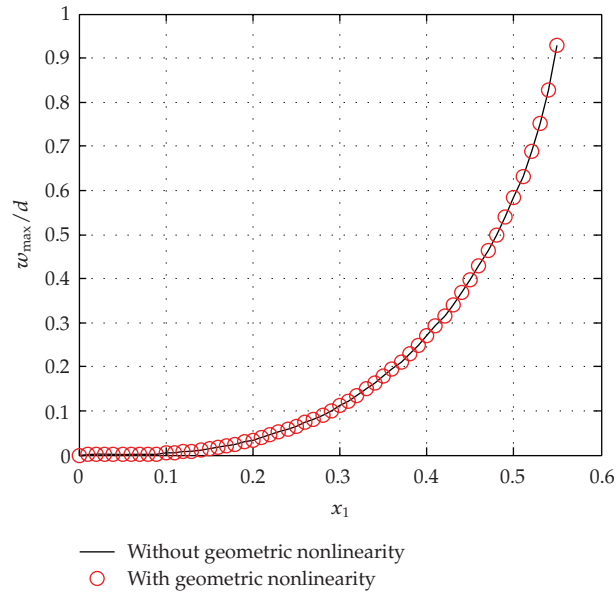
Figure 9: The normalized maximum deflection of the cantilever microbeam versus the normalized liquid distribution with ($\alpha_1 = 0.16$) and without ($\alpha_1 = 0$) including the geometric nonlinearity. Here α_2 is equal to 27.17.
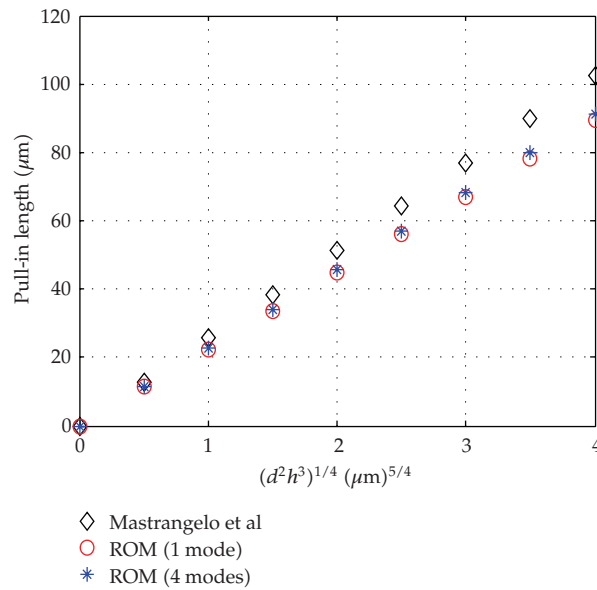

Figure 10: The pull-in length of the cantilever microbeam as a function of the parameter $\left(d^2h^3\right)^{1/4}$.

nature of the used symmetric and antisymmetric mode shapes. Similar behavior has been reported for the convergence of a reduced-order model of microbeams under electrostatic forces [24]. It is also noticed that the microbeam exhibits collapse instability at a specific threshold of liquid volume, as predicted also by Mastrangelo and Hsu [19] for cantilever microbeams.
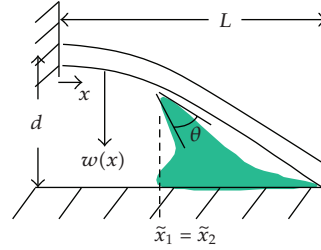
Figure 11: Schematic of a cantilever microbeam under the effect of capillary forces in the pinned configuration.

(a) $\alpha_1 = 6$ and $\alpha_2 = 9.5$.
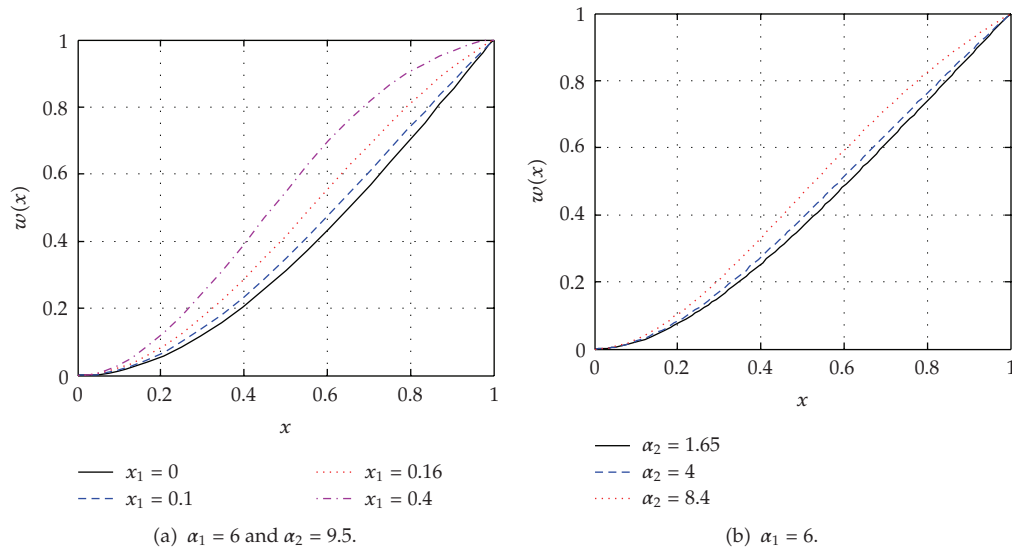
(b) $\alpha_1 = 6$.

Figure 12: The normalized beam deflection versus the normalized beam length using the shooting technique for the case of a hinged boundary condition (a) for different capillary force distributions (b) for a completely wetted beam ($x_1 = 1$) and various values of α_2.

Next, we study the influence of the geometric nonlinearity of the cantilever beam. Figure 9 shows a comparison between the linear and the nonlinear models. The figure shows negligible effect of the geometric nonlinearity on the response of the microbeam. This can be attributed to the small deflection that the microbeam undergoes, compared to its length, before collapsing due to capillary forces, which is not enough to make the weak geometric nonlinearity influential.

Figure 10 shows comparisons between the obtained pull-in lengths using the ROM employing one and four modes to those found by Mastrangelo and Hsu [19] for the case of a cantilever microbeam. Using one mode in this case seems to yield reasonable results, although not accurate as the converged four-mode results. However, Figure 10 shows differences between the pull-in lengths calculated using the ROM and those calculated using the model of Mastrangelo and Hsu [19]. This is similar to the observation made in Figure 6. This might raise a question about the convergence of the Ritz technique of Mastrangelo and Hsu [19]. More investigation about this point needs to be conducted in future research.

4. Modeling of the Collapse Instability of a Cantilever Microbeam from the Pinned to the Adhered Configuration

It is a well known fact in the stiction literature that when a cantilever microbeam collapses to the substrate, due to shock, capillary, or electrostatic forces, its tip tends first to pin to the substrate [16–18]. In its new clamped-pinned configuration, if its restoring force can resist the opposing attractive forces toward the substrate, such as capillary, van der Walls, and electrostatic, it stays in this configuration. Otherwise, it will collapse, in which case part of the cantilever adheres to the substrate [16–18]. In this section, we study the collapse problem of a cantilever microbeam due to a capillary force from the pinned to the adhered configuration. To the best of the author's knowledge, this problem has not been analyzed in the literature. However, similar problems have been studied for the case of cantilever beams actuated by electrostatic forces, for example [16].

In the next analysis, we will assume that the microbeam has been brought down to the substrate by the action of a generic force, which can be electrostatic, capillary, or shock force. No attempt has been made to relate the results of this section to those of Section 3.2. In other words, we treat the problems of Section 3.2 and Section 4 as two separate problems. More advanced model is needed to predict the transition from the configuration of Figure 7 to that of Figure 11, which accounts for the change of the shape of fluid trapped underneath the beam while making the transition and the inertia of the beam.

Because the cantilever beam in this case will be almost in a clamped-pinned configuration, the effect of the geometric nonlinearity (mid-plane stretching) needs to be accounted for [27]. Hence, the nondimensional static equation governing the deflection of the cantilever microbeam under capillary forces in the pinned configuration (Figure 11), and its boundary conditions are given by

$$\frac{\partial^4 w}{\partial x^4} = \alpha_1 \int_0^1 \left(\frac{\partial w}{\partial x} \right)^2 dx \frac{\partial^2 w}{\partial x^2} + \frac{\alpha_2}{(1-w)} u(x - (1 - x_1)), \tag{4.1}$$

$$w(0) = 0, \qquad \frac{\partial w}{\partial x}(0) = 0, \qquad w(1) = 1, \qquad \frac{\partial^2 w}{\partial x^2}(1) = 0, \tag{4.2}$$

where α_1 and α_2 are given by (2.5) and $x_1 = 1 - \tilde{x}_1/L$. In the above model, the effect of the van der Waals forces in close proximity to the substrate has been neglected.

In this case, we use a shooting technique [1] to solve the nonlinear equation. In this method, an initial guess is assumed for the displacement, w, from which the integral term in (4.1), $\Gamma = \int_0^1 (\partial w/\partial x)^2 dx$, is calculated. Then, the nonlinear boundary-value problem, (4.1) and (4.2), with the constant Γ is solved numerically for w using a finite-difference boundary-value solver. A new value of Γ is then calculated based on the obtained w. This procedure is repeated until convergence for the value of Γ is achieved.

As an example, we consider a cantilever microbeam of a gap width underneath and a thickness equal $1\,\mu$m for each. The influence of varying the capillary force distribution and the parameter α_2 on the cantilever microbeam profile is illustrated in Figure 12. It is evident from the figure that when the capillary force distribution x_1 and the parameter α_2 (i.e., the length of the microbeam) increase, the possibility of the microbeam to undergo a structural instability from pinned to adhered configuration increases. Hence, either the length of the microbeam, which is described by the parameter α_2, or the volume of trapped liquid underneath can be taken as a control (bifurcation) parameter in studying the structural
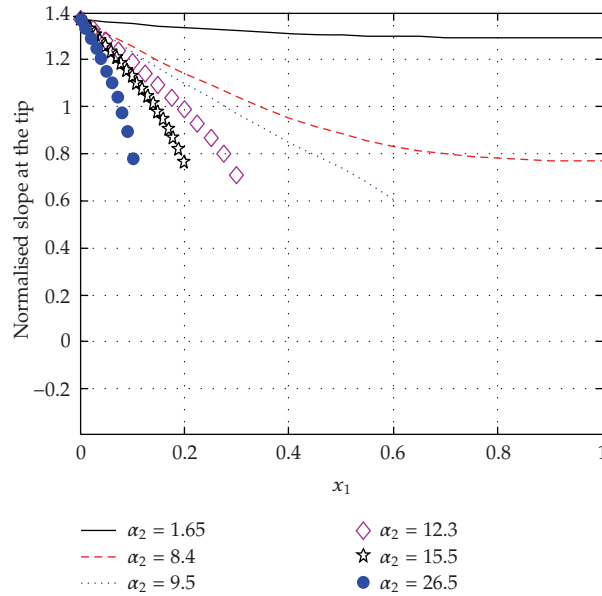
Figure 13: Variation of the normalized slope at the cantilever tip versus the normalized capillary force distribution using the shooting technique for various values of α_2. Here α_1 is equal to 6.
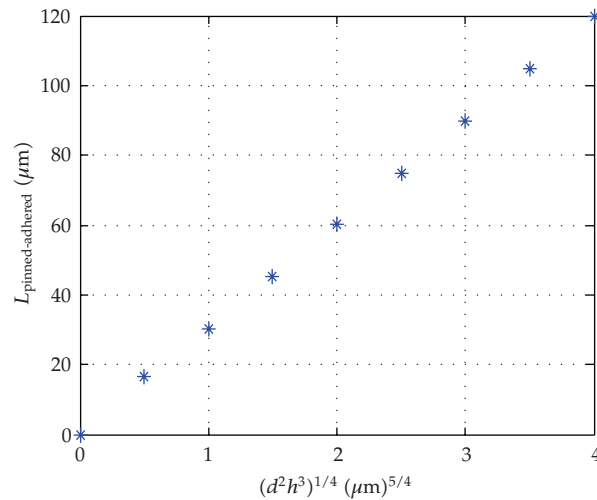

Figure 14: The cantilever critical lengths from the pinned to adhered configuration as function of the parameter $(d^2 h^3)^{1/4}$.

stability of the microbeams. One method to monitor the transition from the pinned to the adhered configuration is to observe the displacement slope at the microbeam tip when varying these control parameters. As noticed in Figure 12, as the control parameter increases, the slope decreases until the microbeam collapses to reach the adhered configuration, where the slope is equal to zero.

Figure 13 shows the variation of the cantilever tip slope for different values of α_2. As mentioned previously, the slope at the cantilever tip decreases with the increase of the capillary force (liquid volume). In the case of completely wetted microbeam ($x_1 = 1$), we notice that below $\alpha_2 = 9.5$, which corresponds to a length of 31 μm, the slope saturates at a constant value indicating reaching an equilibrium state in the pinned configuration with no possibility to collapse. This critical beam length separating beams that can withstand capillary forces in the pinned configuration from those that collapse and adhere to the substrate $L_{\text{pinned-adhered}}$ is calculated in Figure 14 as the parameter $(d^2 h^3)^{1/4}$ is varied. We can notice from this figure that this critical length varies linearly as a function of the beam thickness and the gap width underneath the microbeam.

5. Summary and Conclusion

We presented modeling and simulations of the collapse instabilities of doubly clamped and cantilever microbeams under the effect of capillary forces. We modeled this influence by considering the possible configurations that these microbeams can undergo. The first collapse instability, which brings the microbeam from its free configuration to its pinned configuration, was studied using a reduced-order model employing multi-mode shapes of the beams. The critical lengths of microbeams distinguishing the unstuck from pinned beams (pull-in length) were calculated as a function of the beam thickness and gap width underneath. Comparing the reduced-order model results with the analytical results of Mastrangelo and Hsu [19] yielded good agreement for clamped-clamped beams behaving linearly and slight deviation for beams behaving nonlinearly. A slight deviation was also observed for the case of a cantilever beam. This might be attributed to insufficient convergence of the Ritz method used by Mastrangelo and Hsu [19] based on a single trial function. However, this issue warrants further investigation in the future.

We studied also the instability problem of cantilever microbeams from the pinned to adhered configuration, which represents another structural instability. For this case, a shooting technique was used to solve the static nonlinear boundary-value problem. We studied the variation of the slope at the cantilever microbeam tip while varying the distribution of the capillary force and the beam length. We have seen that the slope tends to zero as the capillary force or the beam length increases, indicating reaching the second instability where a microbeam can collapse from the pinned to the adhered configuration.

References

[1] E. M. Abdel-Rahman, M. I. Younis, and A. H. Nayfeh, "Characterization of the mechanical behavior of an electrically actuated microbeam," *Journal of Micromechanics and Microengineering*, vol. 12, no. 6, pp. 759–766, 2002.

[2] H. A. C. Tilmans and R. Legtenberg, "Electrostatically driven vacuum-encapsulated polysilicon resonators—part II: theory and performance," *Sensors and Actuators A*, vol. 45, no. 1, pp. 67–84, 1994.

[3] Y. Zhang and Y.-P. Zhao, "Static study of cantilever beam stiction under electrostatic force influence," *Acta Mechanica Solida Sinica*, vol. 17, no. 2, pp. 104–112, 2004.

[4] R. Maboudian and R. T. Howe, "Critical review: adhesion in surface micromechanical structures," *Journal of Vacuum Science and Technology B*, vol. 15, no. 1, pp. 1–20, 1997.

[5] T. Lam and R. B. Darling, "Physical modeling of MEMS cantilever beams and the measurement of stiction force," *Journal of Modeling and Simulation of Microsystems*, vol. 4, pp. 418–421, 2001.

[6] T. Yu, R. Ranganathan, N. Johnson, N. Yadav, R. Gale, and T. Dallas, "In situ characterization of induced stiction in a MEMS," *Journal of Microelectromechanical Systems*, vol. 16, no. 2, pp. 355–364, 2007.

[7] Z. C. Leseman, S. P. Carlson, and T. J. Mackin, "Experimental measurements of the strain energy release rate for stiction-failed microcantilevers using a single-cantilever beam peel test," *Journal of Microelectromechanical Systems*, vol. 16, no. 1, pp. 38–43, 2007.

[8] W. M. Van Spengen, R. Puers, and I. De Wolf, "The prediction of suction failures in MEMS," *IEEE Transactions on Device and Materials Reliability*, vol. 3, no. 4, pp. 167–172, 2003.

[9] A. A. Savkar, K. D. Murphy, Z. C. Leseman, T. J. Mackin, and M. R. Begley, "On the use of structural vibrations to release stiction failed MEMS," *Journal of Microelectromechanical Systems*, vol. 16, no. 1, pp. 163–173, 2007.

[10] L. L. Mercado, S.-M. Kuo, T.-Y. T. Lee, and L. Liu, "A mechanical approach to overcome RF MEMS switch stiction problem," in *Proceedings of Electronic Components and Technology Conference*, pp. 377–384, 2003.

[11] L. L. Mercado, S.-M. Kuo, T.-Y. T. Lee, and L. Liu, "Mechanics-based solutions to RF MEMS switch stiction problem," *IEEE Transactions on Components and Packaging Technologies*, vol. 27, no. 3, pp. 560–567, 2004.

[12] C. H. Mastrangelo, "Suppression of stiction in MEMS," Center for Integrated Microsystems, Department of Electrical Engineering and Computer Science, University of Michigan, Ann Arbor, Mich, USA, pp. 1–12.

[13] O. Raccurt, F. Tardif, F. A. D'Avitaya, and T. Vareine, "Influence of liquid surface tension on stiction of SOI MEMS," *Journal of Micromechanics and Microengineering*, vol. 14, no. 7, pp. 1083–1090, 2004.

[14] E. E. Jones, K. D. Murphy, and M. R. Begley, "Mechanical measurements of adhesion in microcantilevers: transitions in geometry and cyclic energy changes," *Experimental Mechanics*, vol. 43, no. 3, pp. 280–288, 2003.

[15] J. A. Knapp and M. P. De Boer, "Mechanics of microcantilever beams subject to combined electrostatic and adhesive forces," *Journal of Microelectromechanical Systems*, vol. 11, no. 6, pp. 754–764, 2002.

[16] S. Gorthi, A. Mohanty, and A. Chatterjee, "Cantilever beam electrostatic MEMS actuators beyond pull-in," *Journal of Micromechanics and Microengineering*, vol. 16, no. 9, pp. 1800–1810, 2006.

[17] M. P. de Boer, P. J. Clews, B. K. Smith, and T. A. Michalske, "Adhesion of polysilicon microbeams in controlled humidity ambients," in *Proceedings of the Materials Research Society Symposium*, vol. 518, pp. 131–136, San Francisco, Calif, USA, April 1998.

[18] M. P. de Boer and T. A. Michalske, "Accurate method for determining adhesion of cantilever beams," *Journal of Applied Physics*, vol. 86, no. 2, pp. 817–827, 1999.

[19] C. H. Mastrangelo and C. H. Hsu, "Mechanical stability and adhesion of microstructures under capillary forces—part I: basic theory," *Journal of Microelectromechanical Systems*, vol. 2, no. 1, pp. 33–43, 1993.

[20] C. H. Mastrangelo and C. H. Hsu, "Mechanical stability and adhesion of microstructures under capillary forces—part II: experiments," *Journal of Microelectromechanical Systems*, vol. 2, no. 1, pp. 44–55, 1993.

[21] R. Legtenberg, H. A. C. Tilmans, J. Elders, and M. Elwenspoek, "Stiction of surface micromachined structures after rinsing and drying: model and investigation of adhesion mechanisms," *Sensors and Actuators A*, vol. 43, no. 1–3, pp. 230–238, 1994.

[22] N. Tas, T. Sonnenberg, H. Jansen, R. Legtenberg, and M. Elwenspoek, "Stiction in surface micromachining," *Journal of Micromechanics and Microengineering*, vol. 6, no. 4, pp. 385–397, 1996.

[23] M. I. Younis, E. M. Abdel-Rahman, and A. Nayfeh, "A reduced-order model for electrically actuated microbeam-based MEMS," *Journal of Microelectromechanical Systems*, vol. 12, no. 5, pp. 672–680, 2003.

[24] A. H. Nayfeh, M. I. Younis, and E. M. Abdel-Rahman, "Reduced-order models for MEMS applications," *Nonlinear Dynamics*, vol. 41, no. 1–3, pp. 211–236, 2005.

[25] P. Lambert, *Capillary Forces in Microassembly: Modeling, Simulation, Experiments, and Case Study*, Springer, New York, NY, USA, 2007.

[26] M. R. M. Crespo da Silva and C. C. Glynn, "Non-linear flexural-flexural-torsional dynamics of inextensional beams—I: equations of motion," *Journal of Structural Mechanics*, vol. 6, no. 4, pp. 437–448, 1978.

[27] A. H. Nayfeh and P. F. Pai, *Linear and Nonlinear Structural Mechanics*, Wiley Series in Nonlinear Science, John Wiley & Sons, Hoboken, NJ, USA, 2004.